Journal of Theoretical and Applied Vibration and Acoustics 7(2) 157-181 (2021)

I S A V

Journal of Theoretical and Applied Vibration and Acoustics

journal homepage: http://tava.isav.ir

# Analytical determination of Bouc-Wen friction model of two contacted flat rough surfaces in elastic region

**Hossein Jamshidi** [a,*], **Ali Koochakinejad** [b]

[a] *Ph.D., Department of Mechanical Engineering, Iran University of Science and Technology, Tehran, IRAN*

[b] *Department of Mechanical Engineering, National University of Skill, Tehran, IRAN*

*Research Article*

**ARTICLE INFO**

*Article history:*
Received 14 February 2020

Received in revised form
5 June 2021

Accepted 23 June 2021

Available online 11 July 2021

*Keywords:*
Rough interface

Bouc-Wen

Hysteresis loop

Friction model

**ABSTRACT**

In this paper, the Bouc-Wen friction model parameters of two elastic rough interfaces are determined analytically based on multi-asperity contact theory. To this, the three main contact characteristics parameters of the rough interface, including slippage friction force, slippage displacement limit, and tangential interface stiffness, are determined. According to multi-asperity contact theory, these three main contact characteristics are physically meaningful parameters related to measurable rough surface parameters such as standard deviations of asperity heights, mean radius of asperity summits, and areal density of asperities. The new frictional contact model of the rough interface is produced as a first-order differential equation form. This model is obtained using exponential function curve-fitting on the interface stiffness behavior of the rough interface. Finally, the constant parameters of the Bouc-Wen friction model are related to three main contact characteristic parameters using a first-order differential equation. In other words, this paper proposed an analytical way to establish the Bouc-Wen model by measurable topography parameters of contacted rough surfaces. The capability and application of the proposed model in engineering problems are investigated and validated experimentally.



Nomenclature

| | | | |
|---|---|---|---|
| $R$ | radius of spherical asperity | $\eta$ | combined areal density of asperities |
| $\sigma$ | standard deviations of asperity heights | $A$ | nominal contact area of the rough interface |
| $a$ | radius of asperities contact area | $\Phi(z)$ | probability density function of asperity heights |
| $w$ | penetration depth of contacting asperities | $K_\tau$ | tangential interface stiffness during shear motion |

* Corresponding author:
*E-mail address:* jamshidi_hossein@alumni.iust.ac.ir (H. Jamshidi)

http://dx.doi.org/10.22064/tava.2023.1995725.1223

| | | | |
|---|---|---|---|
| $w_c$ | critical elastic penetration depth | $K_T$ | initial tangential interface stiffness |
| $z$ | height of asperities | $K_S$ | spring stiffness |
| $y, y_c$ | distance between two flat rough surfaces | $Q_L$ | slippage friction force of rough interface |
| $f_H$ | Hertzian normal force of two contacted asperities | $Q_v$ | tangential force of rough interface in the virgin loading phase |
| $F_n$ | constant normal preload of rough interface | $Q_o$ | tangential force amplitude of rough interface |
| $f_\tau$ | tangential friction force of two contacted asperities | $E, G$ | Young's modulus and shear moduli of contacting surface materials |
| $f_{slip}$ | slippage friction force of two contacted asperities | $\vartheta$ | Poisson's ratios of contacting surface materials |
| $x$ | shear relative displacement of two rough surfaces | $\mu$ | friction coefficient |
| $x_{slip}$ | slippage displacement limit of two contacted asperities | | Index $M$ denotes the classical Mindlin solution |
| $x_L$ | slippage displacement limit of rough interface | | Index $v$ denotes the virgin loading phase in the tangential direction |
| $x_o$ | shear relative motion amplitude of rough interface | | Index 1 and 2 are surface numbers |
| $z_l$ | slippage heights limit of asperity in the virgin loading phase | | |

# 1. Introduction

Frictional energy dissipation is observed in many structures, industrial applications, and mechanical systems. It is necessary to mathematically model hysteresis behaviors of contact surfaces as a source of energy dissipation. The phenomenological and physical model may be applied in contact friction modeling [1]. The phenomenological contact model parameters are obtained using the experimental data. The parameters of this model may have no physical meaning and must be identified. Several phenomenological contact models have demonstrated the ability to reproduce the frictional hysteresis behavior of rough interfaces in jointed structures, such as the Lu-Gre model, the Dahl model, the Valanis model, the Iwan model and the Bouc-Wen friction model [2-4]. This approach will generally require partial differential equations [5]. The differential equation-based phenomenological hysteresis models are specially employed to characterize hysteresis non-linearity [5], such as the Bouc-wen friction model, which is used extensively in the frictionally dissipated energy modeling of nonlinear structural vibrations [6-8]. The Bouc-Wen friction model is formulated as a nonlinear differential equation widely used in nonlinear hysteretic modeling [4, 9]. A.E. Charalampakis and V.K. Koumousis [10] proposed an efficient formulation for the response and dissipated energy of Bouc–Wen hysteresis simulation under symmetric cyclic excitation. Identification of Bouc-Wen hysteresis model parameters is a challenge. Due to the

nonlinearity and internal memorize loop of the Bouc-Wen friction model, identifying its parameters is an important and complicated task in engineering applications [11]. Various identification methods are proposed in the literature [12-18]. L.P. Miguel et al. [19] introduced the harmonic balance method to identify Bouc–Wen model parameters in the nonlinear behavior of bolted structures. Lin et al. [20] proposed an effective procedure to predetermine the parameters of linear subsystem and Bouc-Wen parameters based on the harmonic balance method. Then, an iterative alternating procedure is developed to update the estimation of system parameters and hysteretic force. Based on a joint optimization approach, Lin et al. [9] proposed a novel identification method to identify Bouc-Wen hysteretic systems. This study is interested in analytically extracting Bouc-Wen model parameters of two contacted rough surfaces using a physical-based contact model instead of identifying them. In the physical-based model, the dissipated energy of contacted surfaces is determined based on the interaction of surfaces, such as multi-asperity contact theory, which is based on probability and statistical summation of contacted asperities interactions of two nominally flat rough surfaces [21, 22], where there is a distance between the reference planes of two surfaces, which is defined by means of asperity heights of both surfaces [23]. Assuming reference planes of two rough surfaces are parallel, the contact interface can be equivalently represented as contact between a smooth, rigid, flat surface and an elastic rough surface [22, 23], called a single rough surface (SRS) model. In the SRS model, the state of shear relative motion of contacted surfaces is divided into pre-slip and slide state states. In the pre-slip state, some asperities are in the full stick and pre-slip state, while the contact in other asperities is in the slide state [24]. The three main contact characteristics of the rough interface are slippage friction force, slippage displacement limit, and initial tangential interface stiffness, which can be calculated using the superposition of contacting asperity behaviors. This involves applying the statistical method and integration on asperity heights [23], which relates contact characteristics to the standard measurable roughness parameters [23, 25, 26]. The roughness parameters are standard deviations of the asperity heights, mean curvature radius of asperity summit and areal density of asperities.

In this paper, using multi-asperity contact theory, the contact characteristic of the rough interface is obtained by measuring roughness parameters. The interface stiffness behavior is fitted by a simple exponential decay function, in which the constant parameters of the fitted function are related to three contact characteristics. Finally, the constant parameters of the Bouc-Wen model are determined as related to the fitted function parameters. In other words, using measured roughness parameters, the Bouc-wen friction model is established.

Sections of the present paper are as follows: in Section 2, the multi-asperity contact model is introduced, and the analytical formulation to calculate the contact characteristic of the rough interface is derived. In Section 3, a simple differential equation form of a frictionally contact model is proposed, in which the constant parameters of proposed models are related to contact characteristics of the rough interface. In Section 4, the constant parameters of Bouc-Wen friction model parameters are obtained related to contact characteristics. Also, the simulation results of the determined Bouc-Wen friction model are presented. The capability of the determined Bouc-Wen friction model is examined experimentally in Section 5. It is shown that there is excellent agreement between the proposed simulated hysteresis loop and the test measurements. Finally, Section 6 concludes the study.

## 2. Multi-asperity contact theory

In this section, based on multi-asperity contact theory and the use of the SRS model, the three main contact characteristics of the rough interface, such as initial tangential interface stiffness, slippage friction force, and slippage displacement limit, are extracted. Moreover, the tangential interface stiffness behavior during shear motion is simulated. In the SRS model, it is assumed that the surface asperity shapes are spherical, having the same radius approximately, where for a wide range of asperity heights, an average value can be attributed to the radius of curvature of asperities [27]. The contact of asperities is considered summit to summit approximately, and each asperity from a surface is contacted only by one asperity of the other surface. The elasticity of contacting materials does not differ much, such as contact of two metallic materials, and also, the geometry of asperities does not change due to their elastic deformations, and the deflection (bending) of asperities doesn't take place. The dynamic behavior and inertia of asperities are neglected, and the motion occurs in a quasi-static state. It is noted that the measured peaks on surface topography are not asperities. It is defined by a fitted curve on the measured roughness profile [28], in which the measured profile consists of roughness on roughness as nanoscale on microscale [29]. In the following, the classical Mindlin solution and SRS model are applied in the multi-asperity contact model [24], where the contact interface can be modeled as a contact of a rigid flat surface and a combined elastic rough surface, as shown in Fig**. 1** [23].

In the SRS model, the combined rough interface parameters as standard deviations of asperity heights ($\sigma$), combined radii of asperities ($\bar{R}$) and areal density of asperities ($\eta$) are calculated by combining two contacting surfaces' roughness profiles [30]. Also, asperity heights' distribution function can be determined using roughness parameters such as kurtosis and skewness [31]. Various asperity heights' distribution functions are introduced in the literature; a Gaussian probability density function of asperity heights is as follows [21]:

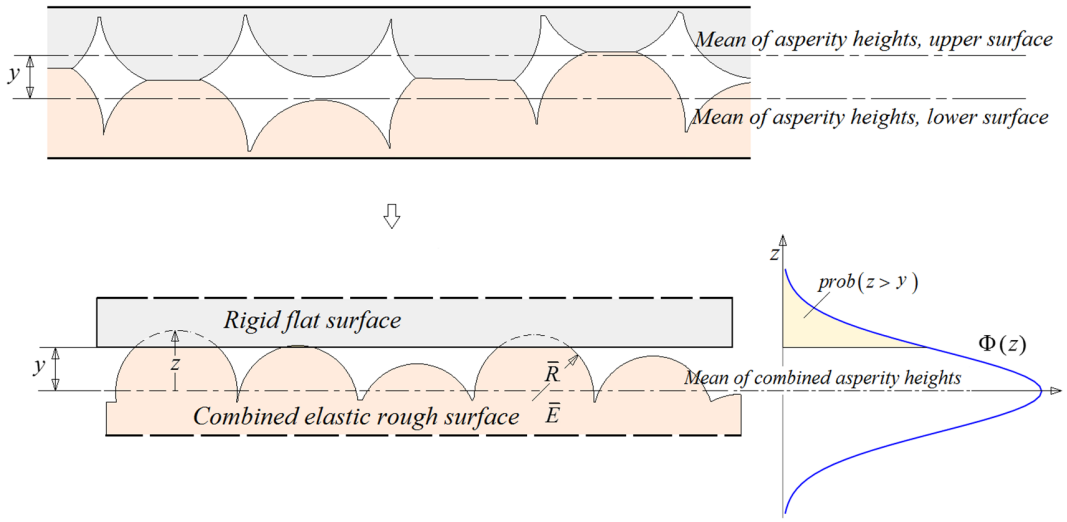


**Fig. 1**. Rough interface and distribution of asperity heights of SRS contact model

$$\Phi(z) = \frac{1}{\sqrt{2\pi}\sigma} e^{-\frac{1}{2}\left(\frac{z}{\sigma}\right)^2}, \qquad (z = z_1 + z_2,\ \ \sigma^2 = {\sigma_1}^2 + {\sigma_2}^2). \tag{1}$$

The parameters $z$ and $\sigma$, are the sum of asperity heights and combined standard deviations of asperity heights of two contacted rough surfaces, respectively. The standard deviations of asperity heights of each surface are designated by $\sigma_1, \sigma_2$. If the distance between two flat surfaces is displayed by $y$, the penetration depth of each contacted asperities will be equal to:

$$w = z - y. \tag{2}$$

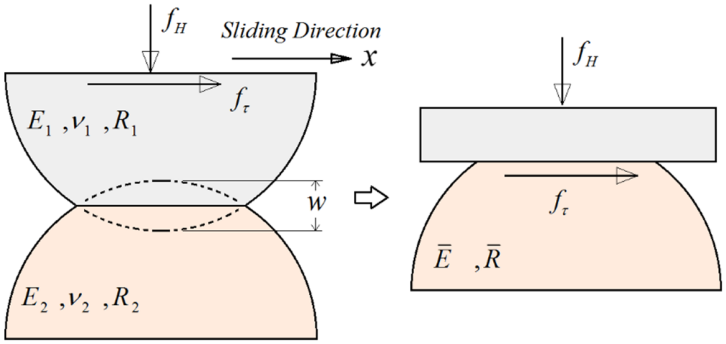


**Fig. 2**. Two contacting spherical particles and their equivalent reduced contact model.

The critical interference, $w_c$ which defines the inception of elastic-plastic contact, is given by [31]:

$$w_c = \left(\frac{\pi \Omega H}{2\bar{E}}\right)^2 \bar{R}, \qquad \Omega = 0.454 + 0.41\vartheta. \tag{3}$$

When the normal interference $w < w_c$, the contact is deemed purely elastically deformed. The normal contact force is assumed to be low, where the deformation of mostly asperities is lower than $w_c$. Therefore, the deformation of the roughness remains in the elastic range, and Hertz's theory is valid for the deformation ranges. This assumption is according to actual behavior in structural vibration problems; after initial high plastic deformations of asperities, rough interface vibrations occur in elastic mode, where the asperity heights decrease and the summit radii of asperities increase [22]. Therefore, the topography parameters of contacting surfaces are measured after the interfaces are exposed to vibrational loadings. Otherwise, a new surface would undergo plastic deformation of asperities at the outset but would run in so that the asperities were just at the elastic deformation limit [32]. Many studies show that the assumption of asperity elastic deformation is valid for structural vibration problems [33, 34].

As shown in Fig. **2**, the contact of two spherical asperities is reduced to the contact of a rigid plane and the spherical body, which has a combined equivalent parameter. The normal force between two asperities with a penetration depth of $w$, is defined using the Hertz relation as follows [22]:

$$f_H = Kw^{1.5}, \qquad K = \frac{4}{3}\bar{E}\sqrt{\bar{R}}, \tag{4}$$

where:

$$\bar{E} = \left((1-\vartheta_1{}^2)E_1{}^{-1} + (1-\vartheta_2{}^2)E_2{}^{-1}\right)^{-1}, \qquad \bar{R} = \left(R_1{}^{-1} + R_2{}^{-1}\right)^{-1}. \tag{5}$$

The Young moduli and Poisson's ratio of asperities are designated by $E_1, E_2$ and $\vartheta_1, \vartheta_2$, respectively. The radius of asperity summits related to two surfaces is denoted by $R_1$ and $R_2$. The relation of total normal preload and the distance between two rough surfaces can be calculated as [22]:

$$F_n(y) = K\eta A \int_y^{\bar{z}_{max}} (z-y)^{1.5} \Phi(z), \tag{6}$$

where $\bar{z}_{max} = 3\sigma$ and is selected as it includes 99.73% of all asperities' height. The combined density of asperities distributed over the nominal area of $A$ is denoted by η. Equation (6) is based on uniformly distributed normal preload on the rough interface. By consideration of pre-known constant normal load $F_n(y) = F_v$, the constant distance of two surfaces ($y = y_c$) can be determined. In tangential direction, the classical Mindlin formulation of friction force in the pre-slip state of the virgin loading phase is as [35]:

$$f_\tau(x) = \mu f_H \left(1 - \left(1 - \frac{16a\bar{G}}{3\mu f_H} x\right)^{1.5}\right). \tag{7}$$

In Equation (7), $\mu$ and $x$ are the friction coefficient and the relative tangential motion, respectively, and $\bar{G}$ is combined shear moduli defined as:

$$\bar{G} = \left((2-\vartheta_1){G_1}^{-1} + (1-\vartheta_2){G_2}^{-1}\right)^{-1}. \tag{8}$$

The shear moduli of two materials are designated by $G_1, G_2$. Parameter $a$ denotes the radius of the contact area, which is defined as:

$$a = \sqrt{\bar{R}w}. \tag{9}$$

In the following, it is assumed that two asperities are of similar material properties and identical summit radius, i.e.:

$$\begin{aligned} &R_1 = R_2 = R, \qquad \vartheta_1 = \vartheta_2 = \vartheta. \\ &E_1 = E_2 = E, \qquad G_1 = G_2 = G. \end{aligned} \tag{10}$$

Then it can be written:

$$\bar{E} = \frac{1}{2}E(1-\vartheta^2)^{-1}, \bar{G} = \frac{1}{2}G(2-\vartheta)^{-1}, E = 2G(1+\vartheta). \tag{11}$$

By substitution Equations (4) and (9) in Equation (7), the tangential force-displacement relation of two contacting spherical particles in pre-slip and slid state can be rewritten as:

$$\begin{aligned} &Preslip\ state\text{:}\ f_\tau(x) = \mu K w^{1.5}\left(1 - \left(1 - \frac{x}{\lambda w}\right)^{1.5}\right), \qquad \lambda = \frac{\mu}{2}\left(\frac{2-\vartheta}{1-\vartheta}\right). \\ &Slide\ state\text{:}\ f_{slip} = \mu K w^{1.5}. \end{aligned} \tag{12}$$

According to Equation (12), the general form of friction force-displacement relation in pre-slip motion is written as:

$$\boldsymbol{f_\tau}(x) = f_{slip}\left(1 - \left(1 - \frac{x}{\boldsymbol{x_s}}\right)^{1.5}\right). \tag{13}$$

The maximum pre-slip limit in the contact of two asperities based on the classical Mindlin solution $x_{slip,M}$, occurs when:

$$f_\tau(x_{slip,M}) = f_{slip}, \tag{14}$$

where $x_{slip,M}$ can be obtained as:

$$x_{slip,M} = \lambda(z - y_c). \tag{15}$$

Therefore, for the classical Mindlin solution, $\boldsymbol{x_s} = x_{slip,M}$ and the tangential force-displacement relation can be rewritten as:

$$f_{\tau,M}(x) = f_{slip}\left(1 - \left(1 - \frac{x}{x_{slip,M}}\right)^{1.5}\right). \tag{16}$$

The total tangential friction force of the rough interface in the pre-slip state, in the virgin loading phase, can be calculated as [23]:

$$Q_{v,M}(x) = \eta A \int_{y_c}^{\bar{z}_l} f_{slip}(z)\Phi(z)\,dz + \eta A \int_{\bar{z}_l}^{\bar{z}_{max}} f_{\tau,M}(x,z)\Phi(z)dz. \tag{17}$$

The $\bar{z}_l$ denote the boundary of asperity heights for slip and stick state and can be determined by equilibrium equation by equating the stick and slip forces ($f_{\tau,M}(\bar{z}_l) = f_{slip}(\bar{z}_l)$). As shown in Fig. **3**, when $z > \bar{z}_l$, the two asperities are in stick (pre-slip state); otherwise, they are in slip (slid state).

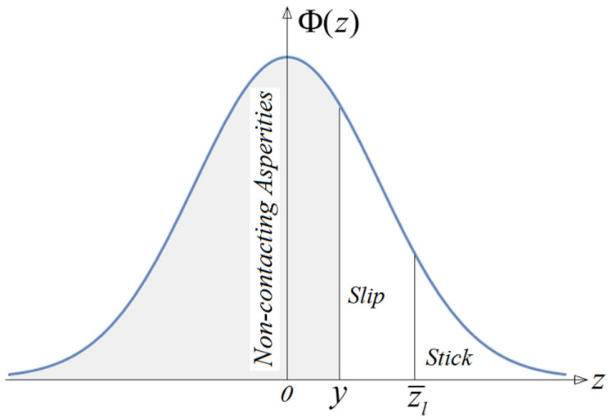


**Fig. 3**. Categories of asperities in the virgin loading phase based on their height distribution.

Generally, the contact friction force in the oscillatory loading phase includes unloading and reloading phases as a hysteresis loop, which can be obtained by integrating pre-slip and slide state friction force of asperities [24]. In the constant normal load, the motion condition and hysteresis loop can be calculated using the Masing rule [36]. The total slippage friction force of the rough interface occurs when all contacted asperities are in a sliding state on the other hand, when $\bar{z}_l = \bar{z}_{max}$. Then the total slippage friction force can be written as:

$$Q_L = \eta A \int_{y_c}^{\bar{z}_{max}} f_{slip}(z)\Phi(z)dz. \tag{18}$$

With respect to Equation (6), can be simplified as:

$$Q_L = \mu F_v. \tag{19}$$

By considering Equations (17) and (18), the slippage displacement limit of a whole rough interface denoted by $x_{L,M}$, will be obtained by solving the following equation:

$$Q_{v,M}(x_{L,M}) = Q_L. \tag{20}$$

Equation (20) is satisfied when the highest asperity slide. Concerning Equation (12), the equilibrium equation of the slippage displacement limit of the whole rough interface can be written as:

$$f_{\tau,M}(x_{L,M}, \bar{z}_{max}) = f_{slip}(\bar{z}_{max}), \tag{21}$$

which leads to:

$$x_{L,M} = \lambda(\bar{z}_{max} - y_c). \tag{22}$$

For the classical Mindlin solution of Equation (16), the tangential stiffness of two contacting asperities can be calculated as follows:

$$k_{\tau,M}(x,z) = \frac{\partial f_{\tau,M}(x,z)}{\partial x} = 1.5\frac{f_{slip}}{x_{slip,M}}\left(1 - \frac{x}{x_{slip,M}}\right)^{0.5}. \tag{23}$$

The total tangential stiffness of the rough interface can be obtained using Equation (17) as follows:

$$K_{\tau,M}(x) = \eta A \int_{\bar{z}_l}^{\bar{z}_{max}} k_{\tau,M}(x,z)\Phi(z)dz. \tag{24}$$

At the beginning of the initial tangential elastic deformation of pre-slip motion ($x = 0$), the initial interface stiffness can be calculated as:

$$K_{T,M} = K_{\tau,M}(x)\big|_{x=0} = 1.5\eta A \int_{y_c}^{\bar{z}_{max}} \frac{f_{slip}(z)}{x_{slip,M}(z)}\Phi(z)dz. \tag{25}$$

Equation (25) can be simplified as:

$$K_{T,M} = 8\bar{G}\eta A\sqrt{\bar{R}} \int_{y_c}^{\bar{z}_{max}} (z - y_c)^{0.5}\Phi(z)dz. \tag{26}$$

The $K_{T,M}$ is defined as the initial tangential interface stiffness of a rough interface based on the Mindlin solution.

Numerous experimental and analytical studies have shown that the Mindlin solution's interface stiffness of rough interface is overestimated [37-39]. C.S. Sandeep and K. Senetakis [38] investigated the contact of spherical particles experimentally. They proposed a new formulation for calculating the upper slippage displacement related to normal load, material, and geometric properties of spherical particles. M. Gonzalez-Valadez et al. [40] investigated the tangential interface stiffness in rough contacts using ultrasonic waves and compared it with existing literature models. Additionally, it is experimentally shown that the tangential stiffness of rough surfaces determined by classical Mindlin solution with Gaussian distribution of asperity heights is higher than actual interface tangential stiffness. The actual stiffness is about $0.5K_{T,M}$ in an investigated case study, where it is understood from the presented test data [31]. Many reviews on the frictionally rough interface proposed the tangential interface stiffness formulation [41-43]. A. Baltazar et al. [42] proposed a correction coefficient for tangential stiffness defined by the Mindlin solution. Baltazar et al. [42] presented tangential stiffness as $\beta K_{T,M}$, where $\beta$ is correction factors accounting for the geometrical misalignments concerning shear directions, which $\beta < 1$ and is

varying between 0.6 and 0.8 for a specific case study. Additionally, using different representations for the surface roughness, the following expression for the tangential stiffness in a rough contact is proposed as [41, 44, 45]:

$$K_T = \Upsilon\left(\frac{F_v}{\sigma}\right), \tag{27}$$

where $\Upsilon$ is a function of Poisson's ratio and interface roughness parameters. Considering the exponential distribution of asperity heights, $\Upsilon$ will equal [44]:

$$\Upsilon = \frac{2(1-\vartheta)}{(2-\vartheta)}. \tag{28}$$

Eriten et al. [46] showed that for light and moderate normal loads, the experimentally measured stiffness values fall very close to the prediction of Equation (27) for studied test specimens. From the reported data in Ref. [46], it can be understood that the nominal normal pressure is less than 2 MPa. According to the literature, the tangential interface stiffness predicted by the Mindlin solution is overestimated. Therefore, the corrected factor should be used to obtain the tangential interface stiffness to achieve an actual interface stiffness. Using Equations (27) and (26), the corrected factor of tangential stiffness $\xi$ is defined as:

$$\xi = \frac{K_T}{K_{T,M}} \quad \xi < 1. \tag{29}$$

According to Equation (29), the actual interface stiffness $K_T$, is lower than classical Mindlin prediction $K_{T,M}$. Similar to Equation (24), the variation of interface stiffness during pre-slip motion can be written as:

$$K_\tau(x) = 1.5\eta A \int_{\bar{z}_l}^{\bar{z}_{max}} \frac{f_{slip}}{\boldsymbol{x_s}}\left(1-\frac{x}{\boldsymbol{x_s}}\right)^{0.5} \Phi(z)dz. \tag{30}$$

Whereas similar to Equation (25):

$$K_T = K_\tau(x)|_{x=0} = 1.5\eta A \int_{y_c}^{\bar{z}_{max}} \frac{f_{slip}(z)}{\boldsymbol{x_s}} \Phi(z)dz. \tag{31}$$

By substitution of Equations (31) and (25) in Equation (29), $\boldsymbol{x_s}$ is determined as:

$$\boldsymbol{x_s} = \xi^{-1} x_{slip,M}. \tag{32}$$

Consequently, the estimated slippage displacement limit of the classical Mindlin solution $x_{L,M}$, is lower than the actual slippage displacement limit denoted by $x_L$. It can be shown that:

$$x_L = \xi^{-1} x_{L,M}. \tag{33}$$

Using Equations (30) and (26), the normalized tangential stiffness is defined as:

$$R(x) = \frac{K_\tau(x)}{K_T}. \tag{34}$$

**Table 1**: Roughness parameters, material properties, and contact interface parameters.

| | | | |
|---|---|---|---|
| Roughness parameter: | $\sigma$ | $\bar{R}$ | $\eta$ |
| Value: | $0.5\mu m$ | $150\mu m$ | $5\times10^{-4}\mu m^{-2}$ |
| Material property: | $E$ | $\vartheta$ | |
| Value: | $200Gpa$ | 0.3 | |
| Contact parameter: | $A$ | $F_n$ | $\mu$ |
| Value: | $500mm^2$ | $50N$ | 0.3 |

As shown in Fig. **4**, the variation of normalized tangential interface stiffness vs normalized pre-slip motion, defined in Equation (34), is plotted using the parameters of Table 1. The pre-slip motion is normalized by the slippage displacement limit $x_L$ of rough interface.

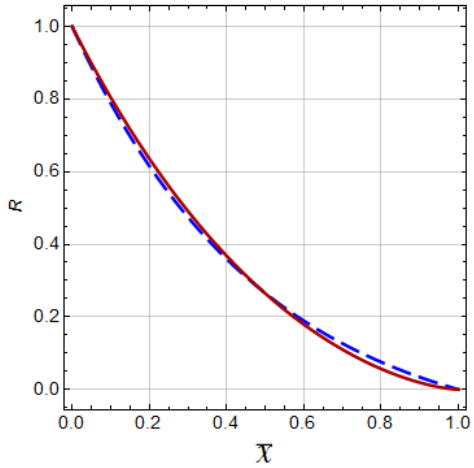


**Fig. 4**. Normalized tangential stiffness variations vs. normalized relative tangential pre-slip motion, resultant stiffness curve (solid line), fitted curve by Equation (38) (dashed line)

In the next section, the differential equation form of the frictionally contact model of an elastic rough interface is derived similarly to the contact model of the hard rough surface and elastic substrate [1].

## 3. Differential equation form of frictionally contact model

In this section, a simple nonlinear differential equation form of the frictionally contact model is introduced based on multi-asperity contact theory, which can simulate the frictionally hysteresis behavior of the rough interface. To this, the tangential stiffness behavior of the rough interface during relative shear motion in the pre-slip state is fitted using the exponential function [1]. The constant parameters of a fitted function are derived using three main constant characteristic parameters of the contact interface, including the initial tangential interface stiffness, slippage friction force, and slippage displacement limit of a rough interface. These parameters are determined using the multi-asperity contact model. As depicted in Fig. **4**, the decreasing behavior of interface stiffness during relative motion can be fitted by function $g(x)$ as:

$$K(x)=\frac{\partial Q_v}{\partial x}=g(x),\quad Q_v(x)|_{x=0}=0. \tag{35}$$

Various functions of $g(x)$ can be fitted on the stiffness curve. Equation (35) describes the relation of stiffness-displacement function from zero initial conditions ($x = 0$ and $Q_v = 0$). The stiffness fitted function must satisfy the following conditions:

$$\begin{aligned} &\text{C-I:} \quad g(0) = K_T. \\ &\text{C-II:} \quad g(x_L) = 0. \\ &\text{C-III:} \quad \int_0^{x_L} g(x)dx = Q_L. \end{aligned} \tag{36}$$

The fitted function must satisfy these three boundary conditions. It is expected that by fitting an exact curve on stiffness curvature, the resulting hysteresis energy will equal the exact amount of contact surface energy dissipation. In this study, the stiffness description function $g(x)$ can be written as a summation of exponential decay functions, in the general case as:

$$g(x) = \sum_{n=0}^{N} \boldsymbol{\Lambda}_n Exp(-\boldsymbol{\Omega}_n|\bar{x}|), \qquad \bar{x} = \frac{x}{x_L}, (\bar{x} \le 1), \tag{37}$$

where $\boldsymbol{\Lambda}_n$ and $\boldsymbol{\Omega}_n$ are constant coefficients. It is interesting to have a simple function with low numbers of constant coefficients needed for determination or identification. The stiffness function must subsequently include three constant parameters for three compatibility relations in Equation (36). Therefore, for a specific case, the fitted curves are assumed to be defined with three parameters of $\boldsymbol{\Lambda}_0$, $\boldsymbol{\Lambda}_1$ and $\boldsymbol{\Omega}_1$ for $N$=1, as:

$$\begin{gathered} \frac{\partial Q_v}{\partial x} = \boldsymbol{\Lambda}_1 Exp(-\boldsymbol{\Omega}_1|\bar{x}|) - \boldsymbol{\Lambda}_0, \qquad Q_v(0) = 0, \qquad (\bar{x} \le 1), \\ \boldsymbol{\Lambda}_0 > 0, \boldsymbol{\Lambda}_1 > 0, \boldsymbol{\Omega}_1 > 0. \end{gathered} \tag{38}$$

The constant coefficient parameters $\boldsymbol{\Lambda}_0$, $\boldsymbol{\Lambda}_1$ and $\boldsymbol{\Omega}_1$ can be calculated by three boundary conditions. By substitution of Equation (38) in Equation (39), the constant coefficient can be calculated using three algebraic equations:

$$\begin{aligned} &\boldsymbol{\Lambda}_1 - \boldsymbol{\Lambda}_0 = K_T. \\ &\boldsymbol{\Lambda}_1 Exp(-\boldsymbol{\Omega}_1) - \boldsymbol{\Lambda}_0 = 0. \\ &\frac{\boldsymbol{\Lambda}_1}{\boldsymbol{\Omega}_1}\left(1 - Exp(-\boldsymbol{\Omega}_1)\right) - \boldsymbol{\Lambda}_0 = \frac{Q_L}{x_L}. \end{aligned} \tag{39}$$

With respect to Equation (39), the parameters of $\boldsymbol{\Lambda}_0$, $\boldsymbol{\Lambda}_1$ and $\boldsymbol{\Omega}_1$ can be obtained related to three main characteristic parameters of frictionally rough interface such as slippage, friction force $Q_L$, slippage displacement limit $x_L$, and initial tangential interface stiffness $K_T$, i.e.:

$$\boldsymbol{\Lambda}_0 = f_1(Q_L, x_L, K_T), \ \ \boldsymbol{\Lambda}_1 = f_2(Q_L, x_L, K_T), \ \ \boldsymbol{\Omega}_1 = f_3(Q_L, x_L, K_T). \tag{40}$$

The fitted stiffness function of Equation (38) is obtained using three main characteristic parameters, calculated using contact parameters of Table 1 normalized to initial stiffness. The results are shown in Fig. **4** and compared with the analytical normalized stiffness function determined by Equation (34), which are in excellent agreement.

Considering the determined parameters of Equation (40), the friction force-displacement relation of the rough interface in the pre-slip state of motion can be obtained using Equation (38). This equation is valid only in the virgin loading phase. With conformity of the Massing rule, Equation (38) can be developed for unloading and reloading phases in all ranges of motions (pre-slip and slide states), as [24]:

$$\frac{\partial Q}{\partial x} = (\boldsymbol{\Lambda}_1 Exp(-0.5\boldsymbol{\Omega}_1 {x_L}^{-1}|x_r|) - \boldsymbol{\Lambda}_0)h(x, x_o),$$
$$Q\big(-x_o.Sign(\dot{x})\big) = -Sign(\dot{x})Q_m. \tag{41}$$

Parameters $h(x, x_o)$ and $Q_m$ are defined in Appendix A. The differential equation form of friction force-displacement relation of Equation (41) describes the fully frictionally hysteresis behavior of the rough interface. The constant coefficient of this model is $\boldsymbol{\Lambda}_0$, $\boldsymbol{\Lambda}_1$ and $\boldsymbol{\Omega}_1$, which are related to $K_T$, $Q_L$ and $x_L$ at the given contact normal preload, using measurement of rough surface parameters $\sigma$, $R$ and $\eta$.

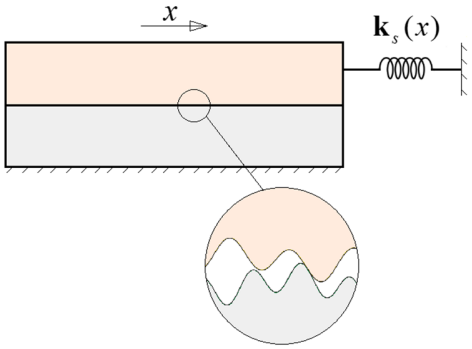


**Fig. 5**. The rough interface with an externally connected parallel spring.

As shown in Fig. 5, when a spring is in parallel to the contact interface, the total force-displacement relation can be written as;

$$\frac{\partial Q^{total}}{\partial x} = \mathbf{k}_s(x) + \frac{\partial Q}{\partial x}. \tag{42}$$

By substitution of the proposed model of Equation (41), the total force of frictionally contact interface can be written as:

$$\frac{\partial Q^{total}}{\partial x} = \mathbf{k}_s(x) + (\boldsymbol{\Lambda}_1 Exp(-0.5\boldsymbol{\Omega}_1 {x_L}^{-1}|x_r|) - \boldsymbol{\Lambda}_0)h(x, x_o),$$
$$Q^{total}\big(-x_o.Sign(\dot{x})\big) = -Sign(\dot{x})Q_m + \int_0^{-x_o Sign(\dot{x})} \mathbf{k}_s(x)dx. \tag{43}$$

In the following, using the differential equation form of Equation (43), which is determined analytically, the Bouc-Wen friction contact model is determined.

## 4. Equivalent Bouc-Wen friction model of rough interface

In this section, the equivalent Bouc-Wen friction contact model of a rough interface is derived. Parameters of the Bouc-Wen model, related to the rough surface, are determined analytically. The general form of the Bouc-Wen friction model is given as [6]:

$$Q^{\mathrm{BW}} = \boldsymbol{k}_l x + \boldsymbol{k}_h z.$$
$$\dot{z} = \dot{x}(\boldsymbol{A} - (\boldsymbol{B}\, Sign(\dot{x}z) + \boldsymbol{C})|z|^{\boldsymbol{N}}), \qquad z(0) = 0, \tag{44}$$

where $Q^{\mathrm{BW}}$ denotes the Bouc-Wen restoring friction force and $\boldsymbol{k}_l$ and $\boldsymbol{k}_h$ are elastic and hysteretic springs, respectively. The linear elastic force and hysteresis friction force are denoted by $Q^e = \boldsymbol{k}_l x$ and $Q^h = \boldsymbol{k}_h z$ [47]. As shown in Fig. **6**, $\boldsymbol{k}_l$ is pre-characterized linear spring stiffness which

is parallel to rough interface. The proposed model in Section 3 is reformulated in the form of the Bouc-Wen model to determine the Bouc-Wen model parameters A, B, C, and N. Concerning Equation (43), when the linear spring with constant stiffness of $\mathbf{k}_l$, is considered parallel to the rough interface, it can be written as:

$$\frac{\partial Q^{total}}{\partial x} = \mathbf{k}_l + (\boldsymbol{\Lambda}_1 Exp(-0.5\boldsymbol{\Omega}_1 {x_L}^{-1}|x_r|) - \boldsymbol{\Lambda}_0)h(x, x_o). \tag{45}$$

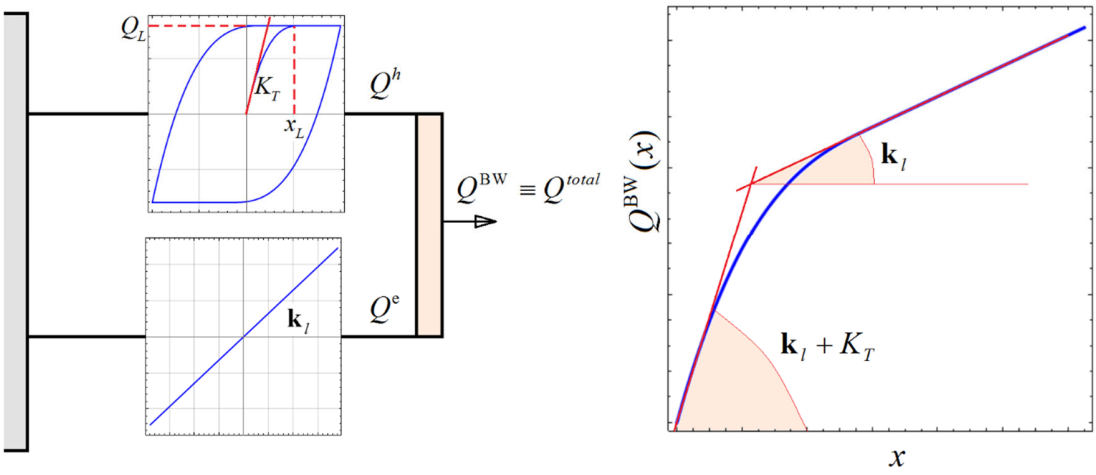


**Fig. 6**. Bouc-Wen friction model.

The second term of Equation (45) defines the hysterias part of friction force, which is defined in Equation (41). Considering $Q^{\mathrm{BW}} = Q^{total}$, the Bouc-Wen model parameters $\boldsymbol{A}$ and $\boldsymbol{B}$, can be obtained as (See Appendix B for further details):

$$\begin{aligned} \boldsymbol{A} &= \left(\frac{\boldsymbol{\Lambda}_1}{2K_T}(\boldsymbol{\Gamma}_1 + \boldsymbol{\Gamma}_2) - \frac{\boldsymbol{\Lambda}_0}{K_T} - Sign(\dot{x})\frac{\boldsymbol{\Lambda}_0\boldsymbol{\Omega}_1}{2K_T x_L}x\right)h(x, x_o), \\ \boldsymbol{B} &= \frac{\boldsymbol{\Omega}_1}{2x_L}h(x, x_o), \end{aligned} \tag{46}$$

where:

$$\boldsymbol{\Gamma}_1 = \left(1 + Exp(-\boldsymbol{\Omega}_1 {x_L}^{-1} x_o)\right). \tag{47}$$

$$\boldsymbol{\Gamma}_2 = \left(1 + Exp(-\boldsymbol{\Omega}_1) + \frac{\boldsymbol{\Lambda}_0\boldsymbol{\Omega}_1}{\boldsymbol{\Lambda}_1}\left(1 - \frac{x_o}{x_L}\right)\right)H(x_o - x_L). \tag{48}$$

It has been noted that $\boldsymbol{k}_h = K_T$, $\boldsymbol{C} = 0$, and $\boldsymbol{N} = 1$. The determined parameters of the equivalent Bouc-Wen model of the rough interface in Equation (44) are related to three constant parameters of $\boldsymbol{\Lambda}_1$, $\boldsymbol{\Omega}_1$,and $\boldsymbol{\Lambda}_0$, that are determined using three main contact characteristic parameters $Q_L$, $K_T$, and $x_L$ in Equations (18), (31) and (33) respectively. These three main contact characteristics are analytically related to surface topography parameters. Therefore, the equivalent Bouc-Wen model of the frictional rough interface can be established analytically by measuring the roughness parameters of $\sigma$, $R$ and $\eta$. For example, using parameters of Table 1, the resultant simulated

hysteresis friction force of equivalent Bouc-Wen model of Equation (44), in pre-slip and slide states of the whole rough interface, is plotted in Fig. **7** for various externally connected spring stiffness. The summary of the determination process of the Bouc-Wen friction model of an elastic frictional rough interface is given in Appendix C.

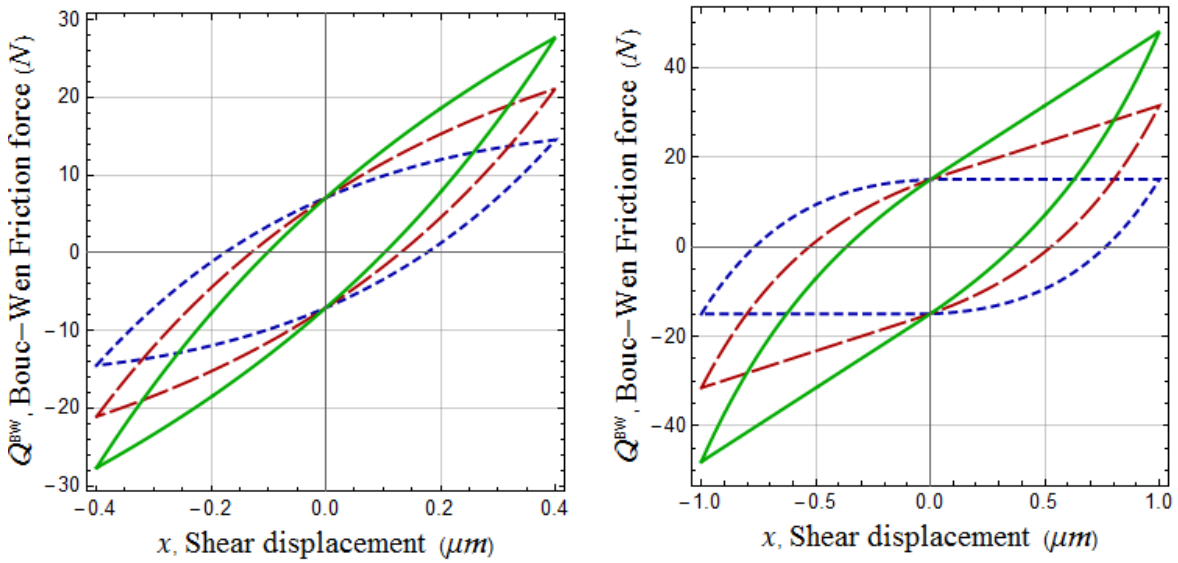


**Fig. 7**. Simulated hysteresis curve by determined Bouc-Wen friction model (short dash line, $\mathbf{k}_l = 0$; long dash line, $\mathbf{k}_l = 0.2K_T$; solid line, $\mathbf{k}_l = 0.4K_T$), a) pre-slip state, b) slide state.

The most important advantage of the Bouc-Wen friction model is modeling the internal memorized hysteresis loop. The following numerical also demonstrates the proposed friction models' capability to simulate hysteresis behavior with nonlocal memory or internal hysteresis loops. Fig. **8** shows the multi-harmonic relative shear motion applied on the rough interface. Based on the parameters of Table 1, the resultant hysteresis friction forces are plotted using the established Bouc-Wen friction model determined in this study.

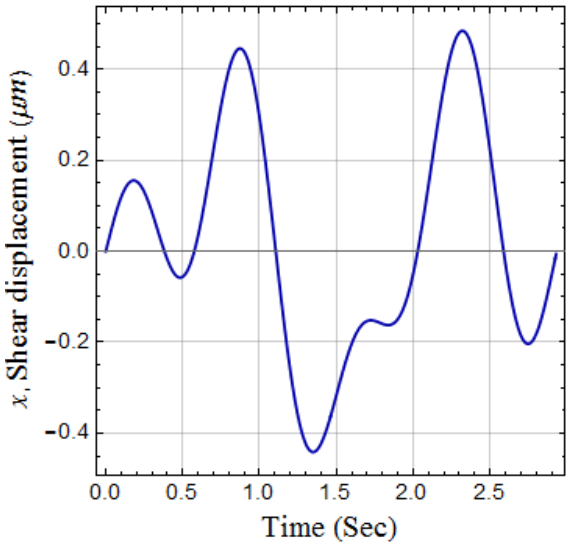


**Fig. 8**. Applied multi-harmonic relative shear motion.

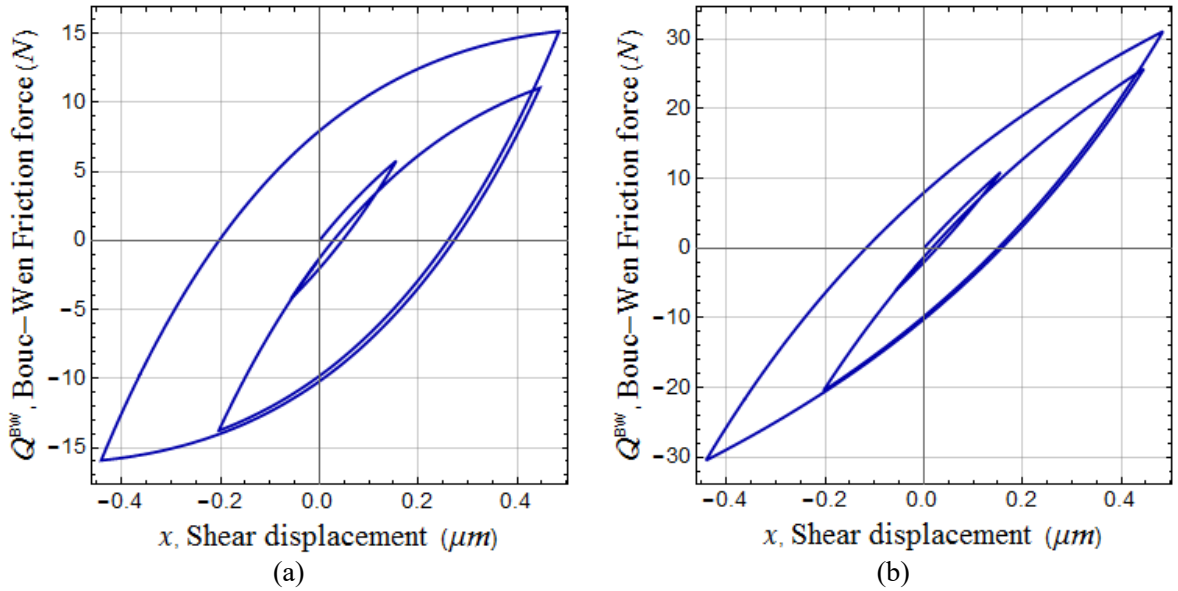


**Fig. 9.** Resultant memorized hysteresis loop due to applied shear motion of Fig. 8, a) $\mathbf{k}_l = 0$, b) $\mathbf{k}_l = 0.4K_T$.

## 5. Application and verification

As shown in Fig. **10** and Fig. **11**, the test setup consists of two aluminum mass blocks with frictional contact. The upper block is attached to a linear spring. It slips on the lower aluminum mass block surface, which is designed similarly to the test setup in previous studies in the literature [1, 48]. The contacting surfaces are carefully machined to achieve a uniform roughness, as specified in Table 2.

**Table 2**: Surface roughness parameters of aluminum block and material properties.

| Parameter: | $\sigma_i$ | $R_i$ | $\eta_i$ | $A$ |
|---|---|---|---|---|
| Value: | $0.8\mu m$ | $170\mu m$ | $250 \times 10^{-6}\mu m^{-2}$ | $77cm^2$ |
| Parameter: | $E$ | $\vartheta$ | S/H | $K_s$ |
| Value: | $70Mpa$ | 0.3 | 0.16 | |

The contact preload equals the weight of the upper block of mass 2 Kg. A suspended B&K mini shaker, Type 4810, excites the mass block. A B&K 8200 force transducer between the moving metal block and the shaker measures the in situ force in the excitation direction throughout the experiments. A DJB A/120/V accelerometer measures the movement of the upper block, and an NI DAQ USB-4431dynamic signal acquisition device is used to condition the measured data.

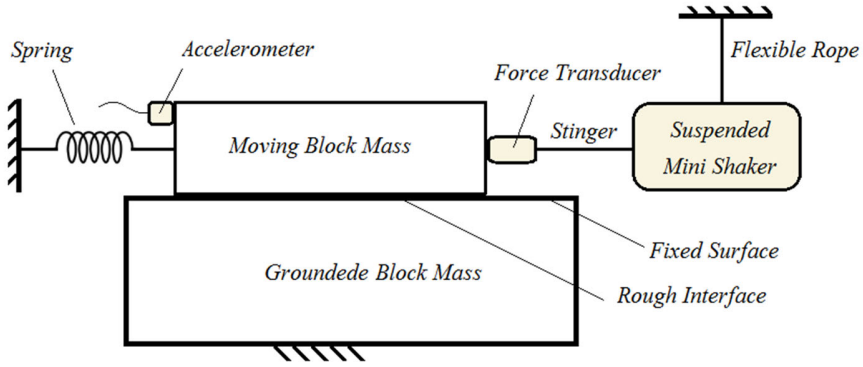


**Fig. 10**. Schematic of the test setup.

The measured response of the test setup to a simple harmonic excitation of 65Hz is shown in Fig. **12**. The Bouc-Wen friction force $Q^{\mathrm{BW}}$ is obtained by subtracting the inertia force of the mass block from the excitation force as:

$$Q^{\mathrm{BW}}(x) = F_{excite} - M\ddot{x}, \tag{49}$$

where:

$$Q^{\mathrm{BW}}(x) = Q(x) + K_S x. \tag{50}$$

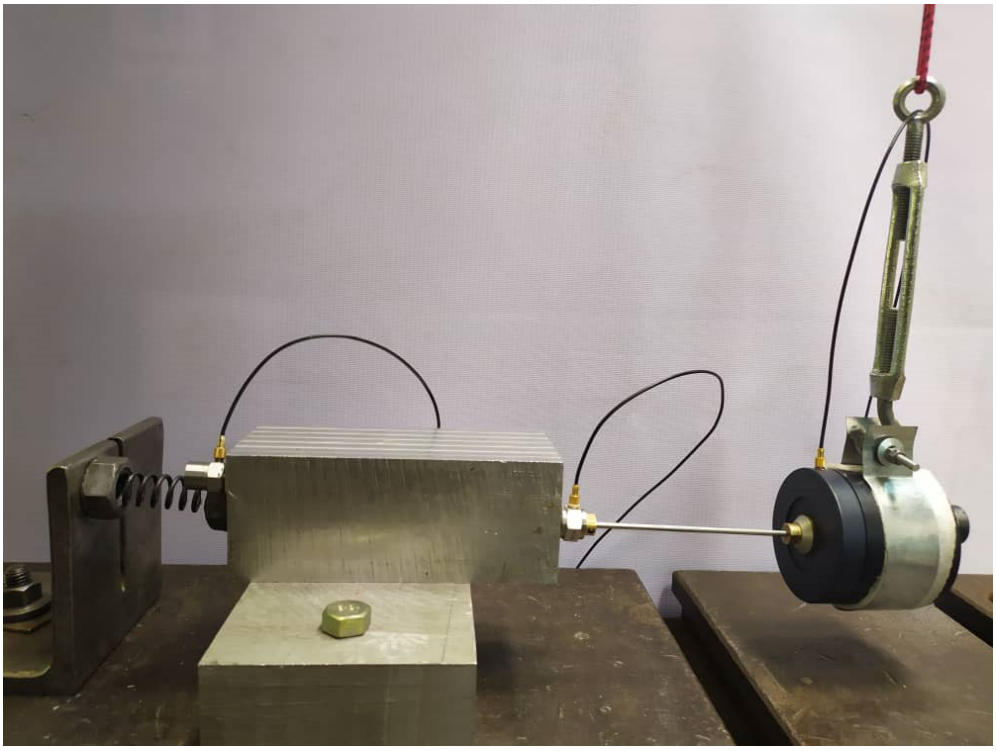

**Fig. 11**. Experimental test setup of the rough interface.

In Equations (49) and (50), $M$ refers to the upper block mass, and the spring stiffness $K_s$ is known. The resultant hysteresis loops of the test setup excite with a simple harmonic force at 65 Hz, and the results are shown in Fig. **13**.

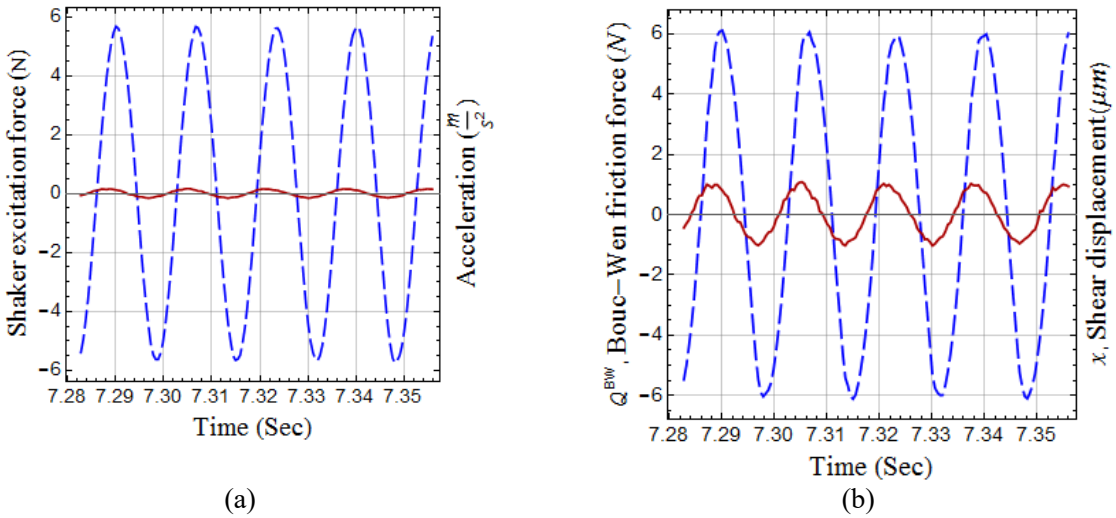


(a) (b)

**Fig. 12**. Time-domain excitation force (dashed line) and metal block shear motion (solid line): (a) Harmonic excitation force, (b) Resultant resistant force (Bouc-Wen friction force).

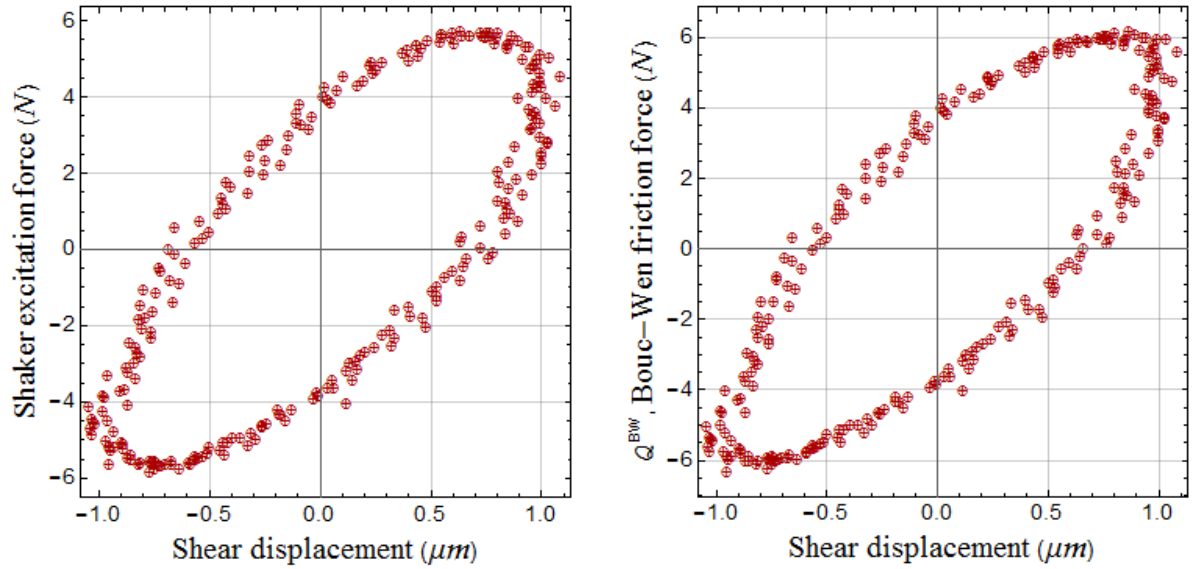


**Fig. 13**. Hysteresis loops: (a) Shaker excitation force at 65 Hz vs. shear motion of upper block, (b) Bouc-Wen Friction force vs. shear displacement (motion).

Experimental results are obtained at the excitation frequency of 65Hz. The shaker applies various excitation force amplitudes, providing various amplitudes of shear relative motion.

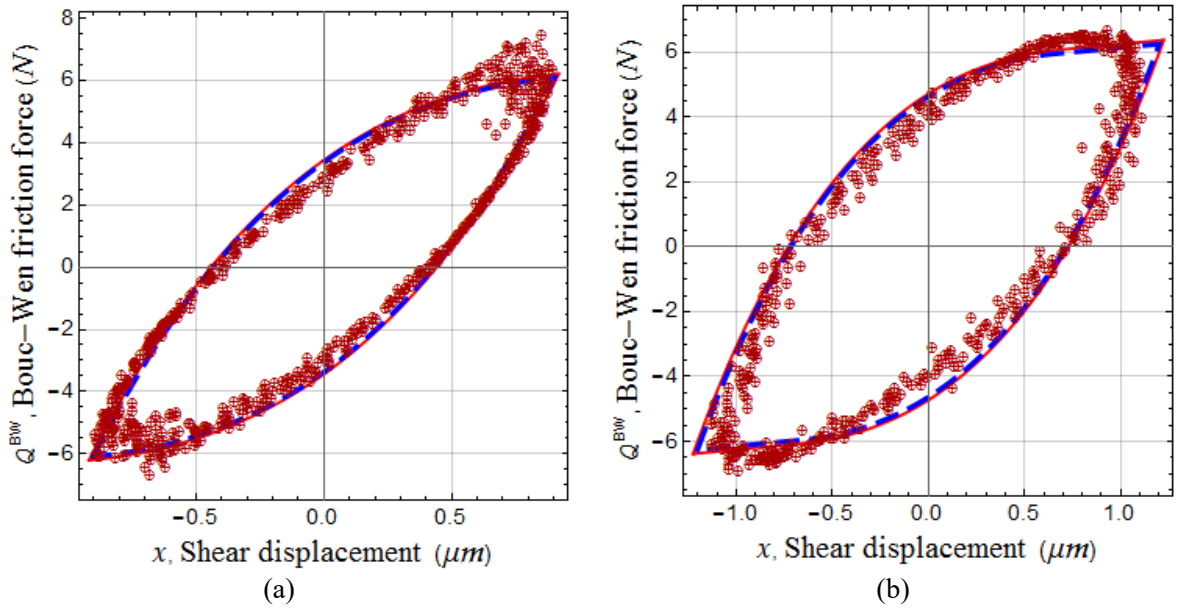


**Fig. 14**. Hysteresis loops of established Bouc-Wen friction model (solid line), rough interface model (dashed line), and the test (⊕) at an excitation frequency of 65 Hz in force amplitudes of (a) 3N, (b) 4N.

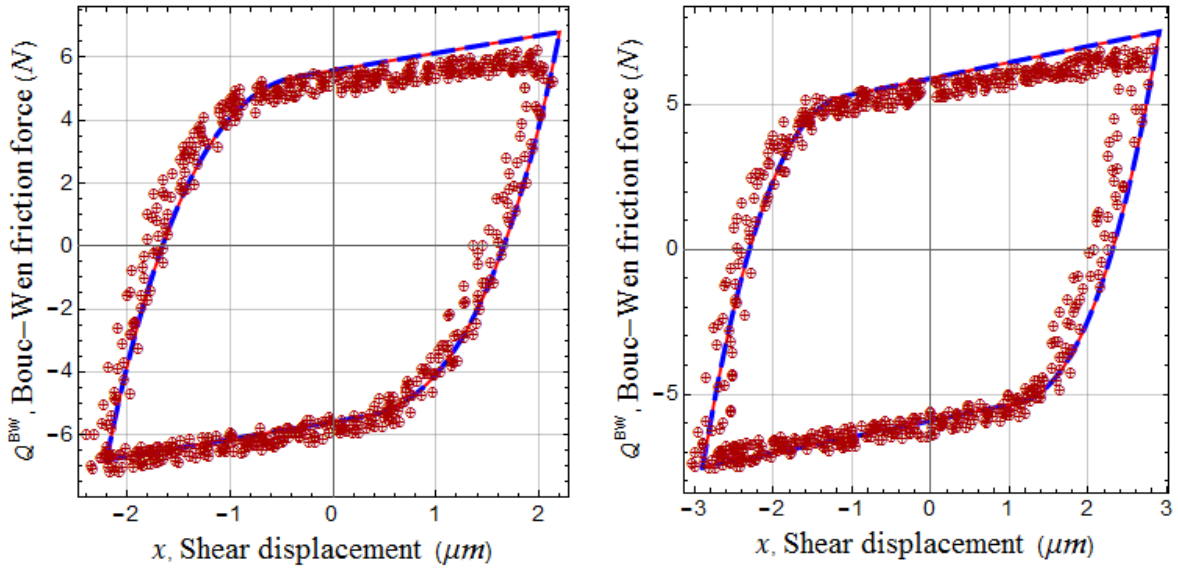


**Fig. 15**. Hysteresis loops of established Bouc-Wen friction model (solid line), rough interface model (dashed line), and the test (⊕) at an excitation frequency of 65 Hz in force amplitudes of (a) 6N, (b) 8N.

The frictional hysteresis curves of the rough interface are determined by the proposed established Bouc-Wen friction model using the roughness parameters of Table 2 and compared with experiment results, as shown in Fig. **14** and Fig**. 15**. These figures demonstrate the results of this validation exercise, indicating excellent agreement between the test observations and the established Bouc-Wen friction model of rough interface. In this test, the roughness parameters of Table 2 are measured after the test is set up and exposed to shaker vibrational excitation. Therefore, the main assumption of the elastic behavior of asperities is almost fulfilled. Additionally, according to the modeling assumption, the uniform distribution of rough interface normal contact force is established entirely by the upper mass, which causes conformity between simulation and experiment. Model simplification is the source of a slight mismatch between analytical and experimental data. Fig. **13** shows that the hysteresis loop is affected by viscous damping in the lower motion amplitude. The insignificant viscous damping of the spring and the test structure is not included in the modeling. Figure 15 shows the higher motion amplitude in the unloading and reloading phases. The spring stiffness is different and has caused the discrepancy in the experiment and simulation results. Also, a slight deviation in the direction of the shaker stinger, which cannot be precisely adjusted, caused the scatter of the test data.

## 6. Conclusion

This paper proposes the new differential equation form of frictionally contact model of rough interface such as two metallic materials contacting surfaces using multi-asperity contact theory in the condition of constant contact normal preload. The differential form of the proposed contact model is defined by constant parameters, which are related to three main contact characteristic parameters of the contact interface: slippage friction force, slippage displacement limit, and initial interface stiffness. These characteristics are calculated analytically by combined roughness profiles. Using the proposed contact model, the Bouc-Wen friction model is determined

analytically. It is shown that the established Bouc-Wen friction model of the rough interface in the elastic region and constant normal load conditions can be applied in frictionally contact applications with excellent accuracy.

## Appendix A

In Equation (41), $h(x, x_o)$ and $Q_m$ , are considered as [1]:

$$\begin{gathered} h(x, x_o) = H[-xSign(\dot{x}) + 2x_L - x_o]. \\ Q_m = Q_o H[x_L - x_o] + Q_L H[x_o - x_L], \\ H[x] = \begin{cases} 1 & x > 0 \\ 0.5 & 0 \\ 0 & x < 0 \end{cases}. \end{gathered} \tag{A. 1}$$

## Appendix B

Concerning the determined virgin tangential loading phase relation defined in Equation (41) and considering the Massing rule [1], the hysteresis friction force of the rough interface for the cyclic loading phases, including the unloading and reloading phases for ($x_o \leq x_L$), can be obtained as:

$$\begin{gathered} Q_{unloading} = -\frac{\boldsymbol{\Lambda}_1 x_L}{\boldsymbol{\Omega}_1}\left(\boldsymbol{\Gamma}_1 - 2Exp\left(-0.5\boldsymbol{\Omega}_1 {x_L}^{-1}(x_o - x)\right)\right) - \boldsymbol{\Lambda}_0 x, \\ Q_{reloading} = \frac{\boldsymbol{\Lambda}_1 x_L}{\boldsymbol{\Omega}_1}\left(\boldsymbol{\Gamma}_1 - 2Exp(-0.5\boldsymbol{\Omega}_1 {x_L}^{-1}(x + x_o))\right) - \boldsymbol{\Lambda}_0 x, \end{gathered} \tag{B. 1}$$

where:

$$\boldsymbol{\Gamma}_1 = \left(1 + Exp(-\boldsymbol{\Omega}_1 {x_L}^{-1} x_o)\right). \tag{B. 2}$$

The compact form of Equation (B. 1) can be written as:

$$Q = Sign(\dot{x})\frac{\boldsymbol{\Lambda}_1 x_L}{\boldsymbol{\Omega}_1}\left(\boldsymbol{\Gamma}_1 - 2Exp(-0.5\boldsymbol{\Omega}_1 {x_L}^{-1}|x_r|)\right) - \boldsymbol{\Lambda}_0 x. \tag{B. 3}$$

By considering linear spring parallel to rough interface with constant stiffness of $\mathbf{k}_s(x) = \boldsymbol{k}_l$, the total tangential force according to Equation (43), will be equal to:

$$Q^{total} = \boldsymbol{k}_l x + Sign(\dot{x})\frac{\boldsymbol{\Lambda}_1 x_L}{\boldsymbol{\Omega}_1}\left(\boldsymbol{\Gamma}_1 - 2Exp(-0.5\boldsymbol{\Omega}_1 {x_L}^{-1}|x_r|)\right) - \boldsymbol{\Lambda}_0 x. \tag{B. 4}$$

Similar to the Bouc-Wen model, the Equation (B. 4) can be divided in terms of elastic and hysteresis terms as:

$$Q^{total} = Q^e + Q, \tag{B. 5}$$

where:

$$\begin{gathered} Q^e = \boldsymbol{k}_l x, \\ Q = Sign(\dot{x})\frac{\boldsymbol{\Lambda}_1 x_L}{\boldsymbol{\Omega}_1}\left(\boldsymbol{\Gamma}_1 - 2Exp(-0.5\boldsymbol{\Omega}_1 {x_L}^{-1}|x_r|)\right) - \boldsymbol{\Lambda}_0 x. \end{gathered} \tag{B. 6}$$

The hysteresis force of $Q$, is considered as:

$$\begin{gathered} Q = K_T z, \\ z = Sign(\dot{x})\frac{\boldsymbol{\Lambda}_1 x_L}{K_T \boldsymbol{\Omega}_1}\left(\boldsymbol{\Gamma}_1 - 2Exp(-0.5\boldsymbol{\Omega}_1 {x_L}^{-1}|x_r|)\right) - \frac{\boldsymbol{\Lambda}_0}{K_T} x. \end{gathered} \tag{B. 7}$$

With respect to Equation (B. 6), it can be derived:

$$Exp(-0.5\boldsymbol{\Omega}{x_L}^{-1}|x_r|) = \frac{1}{\boldsymbol{\Lambda_1}}\frac{\partial Q}{\partial x} + \frac{\boldsymbol{\Lambda_0}}{\boldsymbol{\Lambda_1}}. \tag{B. 8}$$

By substitution of Equation (B. 8) in Equation (B. 7), it can be written:

$$z = Sign(\dot{x})\frac{\boldsymbol{\Lambda_1} x_L}{K_T \boldsymbol{\Omega_1}}\left(\boldsymbol{\Gamma}_1 - 2\left(\frac{1}{\boldsymbol{\Lambda_1}}\frac{\partial Q}{\partial x} + \frac{\boldsymbol{\Lambda_0}}{\boldsymbol{\Lambda_1}}\right)\right) - \frac{\boldsymbol{\Lambda_0}}{K_T}x. \tag{B. 9}$$

Considering $Q = K_T z$ and according to Equation (B. 7), it can be written:

$$\frac{\partial Q}{\partial x} = K_T \frac{\partial z}{\partial x}. \tag{B. 10}$$

By substitution of Equation (B. 10) in Equation (B. 9), it can be obtained:

$$z = Sign(\dot{x})\frac{\boldsymbol{\Lambda_1} x_L}{K_T \boldsymbol{\Omega_1}}\left(\boldsymbol{\Gamma}_1 - 2\left(\frac{K_T}{\boldsymbol{\Lambda_1}}\frac{\partial z}{\partial x} + \frac{\boldsymbol{\Lambda_0}}{\boldsymbol{\Lambda_1}}\right)\right) - \frac{\boldsymbol{\Lambda_0}}{K_T}x, \tag{B. 11}$$

$$\frac{\partial z}{\partial x} = \left(\frac{1}{2}\boldsymbol{\Gamma}_1 - \frac{\boldsymbol{\Lambda_0}}{\boldsymbol{\Lambda_1}}\right)\frac{\boldsymbol{\Lambda_1}}{K_T} - Sign(\dot{x})\frac{\boldsymbol{\Omega_1}}{2x_L}\left(z + \frac{\boldsymbol{\Lambda_0}}{K_T}x\right). \tag{B. 12}$$

Considering that $z = Sign(z)|z|$, it can be written as:

$$\frac{\partial z}{\partial x} = \frac{\boldsymbol{\Lambda_1}}{2K_T}\boldsymbol{\Gamma}_1 - \frac{\boldsymbol{\Lambda_0}}{K_T} - Sign(\dot{x})\frac{\boldsymbol{\Lambda_0}\boldsymbol{\Omega_1}}{2K_T x_L}x - Sign(\dot{x}z)\frac{\boldsymbol{\Omega_1}}{2x_L}|z|. \tag{B. 13}$$

The Equation (B. 13), which is valid for ($x_o \le x_L$), can be rewritten in the form of a time domain as:

$$\begin{gathered}\dot{z} = \boldsymbol{X}_1\dot{x}, \\ \boldsymbol{X}_1 = \left(\frac{\boldsymbol{\Lambda_1}}{2K_T}\boldsymbol{\Gamma}_1 - \frac{\boldsymbol{\Lambda_0}}{K_T} - Sign(\dot{x})\frac{\boldsymbol{\Lambda_0}\boldsymbol{\Omega_1}}{2K_T x_L}x\right) - Sign(\dot{x}z)\frac{\boldsymbol{\Omega_1}}{2x_L}|z|,\end{gathered} \tag{B. 14}$$

where:

$$\dot{z} = \frac{dz}{dt}, \qquad \dot{x} = \frac{dx}{dt}. \tag{B. 15}$$

Similarly, as derived from Equation (B. 1) to Equation (B. 14), for ($x_o > x_L$) it is obtained that:

$$\begin{gathered}\dot{z} = \boldsymbol{X}_2\dot{x}.h(x, x_o), \\ \boldsymbol{X}_2 = \left(\frac{\boldsymbol{\Lambda_1}}{2K_T}\boldsymbol{\Gamma}_2 - \frac{\boldsymbol{\Lambda_0}}{K_T} - Sign(\dot{x})\frac{\boldsymbol{\Lambda_0}\boldsymbol{\Omega_1}}{2K_T x_L}x\right) - Sign(\dot{x}z)\frac{\boldsymbol{\Omega_1}}{2x_L}|z|.\end{gathered} \tag{B. 16}$$

Where:

$$\boldsymbol{\Gamma}_2 = \left(1 + Exp(-\boldsymbol{\Omega_1}) + \frac{\boldsymbol{\Lambda_0}\boldsymbol{\Omega_1}}{\boldsymbol{\Lambda_1}}\left(1 - \frac{x_o}{x_L}\right)\right)H(x_o - x_L). \tag{B. 17}$$

By composing Equation (B. 14) with Equation (B. 16) and keeping in mind that ($h(x, x_o) = 1$), when ($x_o \le x_L$), for all state of motions of pre-slip and slide state, it can be written as:

$$\begin{gathered}\dot{z} = \boldsymbol{X}\dot{x}h(x, x_o), \\ \boldsymbol{X} = \left(\frac{\boldsymbol{\Lambda_1}}{2K_T}(\boldsymbol{\Gamma}_1 + \boldsymbol{\Gamma}_2) - \frac{\boldsymbol{\Lambda_0}}{K_T} - Sign(\dot{x})\frac{\boldsymbol{\Lambda_0}\boldsymbol{\Omega_1}}{2K_T x_L}x\right) - Sign(\dot{x}z)\frac{\boldsymbol{\Omega_1}}{2x_L}|z|.\end{gathered} \tag{B. 18}$$

By substitution of Equation (B. 18) in Equation (B. 5), the established model for both pre-slip and slide state of motions will be equal to:

$$\begin{aligned} Q^{total} &= \boldsymbol{k}_l x + K_T z, \\ \dot{z} &= \boldsymbol{X}\dot{x}. \end{aligned} \tag{B. 19}$$

By comparison of Equation (B. 19) with Equation (44), where ($Q^{\mathrm{BW}} = Q^{total}$), the constant parameters of Bouc-Wen model can be determined as:

$$\boldsymbol{k}_h = K_T, \qquad \boldsymbol{C} = 0, \qquad \boldsymbol{N} = 1, \tag{B. 20}$$

and

$$\begin{aligned} \boldsymbol{A} &= \left(\frac{\boldsymbol{\Lambda}_1}{2K_T}(\boldsymbol{\Gamma}_1 + \boldsymbol{\Gamma}_2) - \frac{\boldsymbol{\Lambda}_0}{K_T} - Sign(\dot{x})\frac{\boldsymbol{\Lambda}_0\boldsymbol{\Omega}_1}{2K_T x_L}x\right) h(x, x_o), \\ \boldsymbol{B} &= \left(\frac{\boldsymbol{\Omega}_1}{2x_L}\right) h(x, x_o). \end{aligned} \tag{B. 21}$$

## Appendix C

The calculation process of determined Bouc-Wen friction model of a rough interface is summarized in the following steps:

**Step 1**: Specifying contacted surface material properties $E, \nu, A$, combined roughness parameters $\sigma, \bar{R}, \eta$ and $\mu$.
**Step 2**: Calculating the distance of the reference plane of two surfaces $y_c$, concerning constant normal interface load $F_y$, using Equation (6).
**Step 3**: Calculation of three main contact characteristic parameters including $Q_L$, $K_T$, and $x_L$ using Equations (18), (31), and (33).
**Step 4**: Calculation of three constant coefficient parameters of $\boldsymbol{\Lambda}_0$, $\boldsymbol{\Lambda}_1$ and $\boldsymbol{\Omega}_1$using Equation (39).
**Step 5**: Calculation of constant parameters of the Bouc-Wen friction model defined in Equation (44), including $\boldsymbol{k}_h, \boldsymbol{C}, \boldsymbol{N}, \boldsymbol{A}$ and $\boldsymbol{B}$, using Equations (B. 20) and (B. 21).

## References

[1] H. Jamshidi, E. Tavakoli, H. Ahmadian, Modeling polymer-metal frictional interface using multi-asperity contact theory, Mechanical Systems and Signal Processing, 164 (2022) 108227.

[2] D.J. SEGALMAN, An Initial Overview of Iwan Modeling for Mechanical Joints, in, United States, 2001, pp. Medium: ED; Size: 55 pages.

[3] L. Gaul, R. Nitsche, The Role of Friction in Mechanical Joints, Applied Mechanics Reviews, 54 (2001) 93-106.

[4] F. Ikhouane, J. Rodellar, Systems with hysteresis: analysis, identification and control using the Bouc-Wen model, John Wiley & Sons, 2007.

[5] Y. Xu, X. Li, X. Yang, Z. Yang, L. Wu, Q. Chen, A two-stage model for rate-dependent inverse hysteresis in reluctance actuators, Mechanical Systems and Signal Processing, 135 (2020) 106427.

[6] M. Ismail, F. Ikhouane, J. Rodellar, The hysteresis Bouc-Wen model, a survey, Archives of Computational Methods in Engineering, 16 (2009) 161-188.

[7] A. Bhattacharjee, A. Chatterjee, Dissipation in the Bouc–Wen model: Small amplitude, large amplitude and two-frequency forcing, Journal of Sound and Vibration, 332 (2013) 1807-1819.

[8] B. Painter, G. Ferrari, M. Amabili, Nonlinear vibrations of beams with Bouc–Wen hysteretic boundary conditions, Nonlinear Dynamics, 108 (2022) 2903-2916.

[9] M. Lin, C. Cheng, G. Zhang, B. Zhao, Z. Peng, G. Meng, Identification of Bouc-Wen hysteretic systems based on a joint optimization approach, Mechanical Systems and Signal Processing, 180 (2022) 109404.

[10] A.E. Charalampakis, V.K. Koumousis, On the response and dissipated energy of Bouc–Wen hysteretic model, Journal of Sound and Vibration, 309 (2008) 887-895.

[11] L. Wang, Z.-R. Lu, Identification of Bouc-Wen hysteretic parameters based on enhanced response sensitivity approach, Journal of Physics: Conference Series, 842 (2017) 012021.

[12] A.E. Charalampakis, V.K. Koumousis, Identification of Bouc–Wen hysteretic systems by a hybrid evolutionary algorithm, Journal of Sound and Vibration, 314 (2008) 571-585.

[13] H. Zhu, X. Rui, F. Yang, W. Zhu, M. Wei, An efficient parameters identification method of normalized Bouc-Wen model for MR damper, Journal of Sound and Vibration, 448 (2019) 146-158.

[14] R. Ceravolo, S. Erlicher, L.Z. Fragonara, Comparison of restoring force models for the identification of structures with hysteresis and degradation, Journal of Sound and Vibration, 332 (2013) 6982-6999.

[15] A. Kyprianou, K. Worden, M. Panet, Identification of hysteretic systems using the differential evolution algorithm, Journal of Sound and vibration, 248 (2001) 289-314.

[16] J.-L. Ha, R.-F. Fung, C.-S. Yang, Hysteresis identification and dynamic responses of the impact drive mechanism, Journal of Sound and Vibration, 283 (2005) 943-956.

[17] R. Manikantan, T. Ghosh Mondal, S. Suriya Prakash, C. Vyasarayani, Parameter identification of Bouc–Wen type hysteresis models using homotopy optimization, Mechanics Based Design of Structures and Machines, 50 (2022) 26-47.

[18] R. Frans, Y. Arfiadi, J. Utomo, Parameter Identification of Bouc-Wen Model Using Firefly Algorithm, in: S. Belayutham, C.K.I. Che Ibrahim, A. Alisibramulisi, H. Mansor, M. Billah (Eds.) Proceedings of the 5th International Conference on Sustainable Civil Engineering Structures and Construction Materials, Springer Singapore, Singapore, 2022, pp. 155-171.

[19] L.P. Miguel, R.d.O. Teloli, S.d. Silva, Bayesian model identification through harmonic balance method for hysteresis prediction in bolted joints, Nonlinear Dynamics, 107 (2022) 77-98.

[20] M. Lin, B. Sun, C. Cheng, B. Zhao, Z. Peng, G. Meng, Alternating state-parameter identification of Bouc-Wen hysteretic systems from steady-state harmonic response, Journal of Sound and Vibration, 538 (2022) 117242.

[21] J.A. Greenwood, J.H. Tripp, The Contact of Two Nominally Flat Rough Surfaces, Proceedings of the Institution of Mechanical Engineers, 185 (1970) 625-633.

[22] J.A. Greenwood, J.P. Williamson, Contact of nominally flat surfaces, Proceedings of the royal society of London. Series A. Mathematical and physical sciences, 295 (1966) 300-319.

[23] M. Eriten, A. Polycarpou, L. Bergman, Physics-based modeling for fretting behavior of nominally flat rough surfaces, International Journal of Solids and Structures, 48 (2011) 1436-1450.

[24] H. Jamshidi, H. Ahmadian, A modified rough interface model considering shear and normal elastic deformation couplings, International Journal of Solids and Structures, 203 (2020) 57-72.

[25] N.N. Balaji, W. Chen, M.R.W. Brake, Traction-based multi-scale nonlinear dynamic modeling of bolted joints: Formulation, application, and trends in micro-scale interface evolution, Mechanical Systems and Signal Processing, 139 (2020) 106615.

[26] W. Zhan, P. Huang, Physics-based modeling for lap-type joints based on the Iwan model, Journal of Tribology, 140 (2018) 051401.

[27] P.R. Nayak, Random Process Model of Rough Surfaces, Journal of Lubrication Technology, 93 (1971) 398-407.

[28] J. Greenwood, J.-J. Wu, Surface roughness and contact: an apology, Meccanica, 36 (2001) 617-630.

[29] A. Majumdar, B. Bhushan, Fractal Model of Elastic-Plastic Contact Between Rough Surfaces, Journal of Tribology, 113 (1991) 1-11.

[30] N. Yu , A.A. Polycarpou, Combining and Contacting of Two Rough Surfaces with Asymmetric Distribution of Asperity Heights, Journal of Tribology, 126 (2004) 225-232.

[31] W. Zhan, P. Huang, Modeling tangential contact based on non-Gaussian rough surfaces, Proceedings of the Institution of Mechanical Engineers, Part J: Journal of Engineering Tribology, 233 (2019) 51-60.

[32] J.F. Archard, Surface topography and tribology, Tribology, 7 (1974) 213-220.

[33] I.I. Argatov, E.A. Butcher, On the Iwan models for lap-type bolted joints, International Journal of Non-Linear Mechanics, 46 (2011) 347-356.

[34] D. Li, D. Botto, C. Xu, M. Gola, A new approach for the determination of the Iwan density function in modeling friction contact, International Journal of Mechanical Sciences, 180 (2020) 105671.

[35] K.L. Johnson, Contact mechanics, Cambridge university press, 1987.

[36] D. Wang, C. Xu, X. Fan, Q. Wan, Reduced-order modeling approach for frictional stick-slip behaviors of joint interface, Mechanical Systems and Signal Processing, 103 (2018) 131-138.

[37] M. Gonzalez-Valadez, A. Baltazar, R. Dwyer-Joyce, Study of interfacial stiffness ratio of a rough surface in contact using a spring model, Wear, 268 (2010) 373-379.

[38] C. Sandeep, K. Senetakis, An experimental investigation of the microslip displacement of geological materials, Computers and Geotechnics, 107 (2019) 55-67.

[39] S. Malamut, Y. Kligerman, I. Etsion, The effect of dwell time on the static friction in creeping elastic–plastic polymer spherical contact, Tribology letters, 35 (2009) 159-170.

[40] M. González Valadez, R.S. Dwyer-Joyce, On the interface stiffness in rough contacts using ultrasonic waves, Ingeniería mecánica, tecnología y desarrollo, 3 (2008) 29-36.

[41] T. Baumberger, C. Caroli, Solid friction from stick–slip down to pinning and aging, Advances in Physics, 55 (2006) 279-348.

[42] A. Baltazar, S.I. Rokhlin, C. Pecorari, On the relationship between ultrasonic and micromechanical properties of contacting rough surfaces, Journal of the Mechanics and Physics of Solids, 50 (2002) 1397-1416.

[43] N. Yoshioka, C.H. Scholz, Elastic properties of contacting surfaces under normal and shear loads: 1. Theory, Journal of Geophysical Research: Solid Earth, 94 (1989) 17681-17690.

[44] S. Medina, D. Nowell, D. Dini, Analytical and numerical models for tangential stiffness of rough elastic contacts, Tribology Letters, 49 (2013) 103-115.

[45] P. Berthoud, T. Baumberger, Shear stiffness of a solid–solid multicontact interface, Proceedings of the Royal Society of London. Series A: Mathematical, Physical and Engineering Sciences, 454 (1998) 1615-1634.

[46] M. Eriten, C.-H. Lee, A.A. Polycarpou, Measurements of tangential stiffness and damping of mechanical joints: Direct versus indirect contact resonance methods, Tribology international, 50 (2012) 35-44.

[47] A. Charalampakis, V. Koumousis, On the response and dissipated energy of Bouc–Wen hysteretic model, Journal of Sound and Vibration, 309 (2008) 887-895.

[48] A. Mahmoodi, H. Ahmadian, Coupling Between the Tangential and Normal Direction in Turbine Blade Forced Vibration Analysis, Journal of Vibration Engineering & Technologies, 10 (2022) 2251-2261.